4

Virtual testing for material formability

S V LOMOV, Katholieke Universiteit Leuven, Belgium

4.1 Introduction

Deformability of textile preforms plays a key role in the quality of a composite part formed into a 3D shape and processed using liquid moulding techniques such as resin transfer moulding (RTM). Ill-chosen placement of the preform, disregarding its behaviour under heavy strain in complex deformation may result in the preform wrinkling or even damage, deteriorating the performance of the composite part. This explains the importance of predictive modelling of deformability of textile preforms. The deformation modes of primary importance are in-plane deformation (tension and shear) and compression of the preform. Deformability of woven preforms in these modes is the subject of the present chapter. Out-of-plane bending may also be considered, as it can affect internal geometry of the preform, especially for small bending radii; a model of the woven fabric bending can be found in refs 1 and 2. Naturally the deformability of woven fabrics is also important for apparel textiles, and has attracted attention of textile materials researchers. Works of Kawabata, Niva and Kawai,[3–5] de Jong and Postle,[6] Hearle and Shanahan[7] have established an approach to mathematical modelling of deformation of woven fabrics, which can be summarised by three principles.

First, the model uses deformations, rather than loads, as input for in-plane deformation (for compression model the applied pressure is the input). An overall deformation pattern is imposed over the woven fabric repeat (unit cell) to change the spacing of the yarns in tension and the angle between them in shear. As formulated by Komori and Ito,[8] the unit cell is subject to transformation of coordinates defined by the given deformation. The contacts between yarns stay unchanged in tension, and experience rotation (not sliding) of the contacting yarns in shear.

Second, the principle of minimum energy is applied to compute the internal geometry of the deformed fabric. With the spacing and orientation of the warp and weft given, the yarn paths are defined using one of available geometrical models (Peirce's, elastica, splines, etc.), with crimp heights and dimensions of

the cross-sections of the yarns (which can change under transversal force caused by tension) as parameters. These parameters are calculated via the principle of minimum total energy, associated with the yarn tension, bending and compression. Tension of the yarn is computed using the experimental tension diagram. Elongation of the yarn is estimated by the difference between yarn length in the repeat before and after the deformation. Experimental bending and compression diagrams are used to compute bending energy and resistance to compression. All these experimental diagrams are non-linear. Application of the principle of minimum energy to fibrous assemblies must be considered as heuristic, as it can be applied rigorously to conservative systems only. This means that frictional effects are not taken into account in the solution of the minimisation problem. The internal friction between fibres in the yarns enters the calculations via non-linear bending and compression diagrams. The inter-yarn friction is absent in tension, and manifests itself in the rotation of the contacting yarns in shear.

Third, the applied loads are computed via the balance between, on one hand, the mechanical work done by the loads on deformations of the unit cell, and, on the other hand, the sum of the change of the total energy of the deformed yarns and the work of friction (if any).

In the papers cited above,[3–7] and some others,[9–14] the approach has been successfully applied to plain woven fabrics. It has also been reported to work for twills and satins.[15] We will use this scheme for all three types of deformation under consideration: compression, bi-axial tension and shear.

Returning to deformability of woven reinforcements for composites, one finds quite a number of publications on modelling. The model complexities range from simple empirical models to elaborate finite element descriptions. Certain important points have been investigated, which were not covered by earlier 'apparel-oriented' models.

In studies of compression the attention was given to compressibility of the reinforcement at high loads, which are characteristic of composite processing. The compression curve is broken into three regions (low, medium and high loads), each dominated by different phenomena.[16–19] The nesting of layers of the reinforcement is taken into account.[17,20,21] Models of shear of woven reinforcements[22–29] have to consider very high shear angles (up to 60–70º) occurring in forming of complex 3D parts. This is dealt with by an introduction of models of lateral compression of the yarns, which come into contact when the shear angle reaches and exceeds the locking angle of the fabric 'trellis'. The simple, but not true-to-life concept of preserving the volume of the unit cell to calculate the change of the thickness of fabric in shear, has been advanced to more correct considerations of yarn compression.

Recently, finite element descriptions of deformability of textiles have been introduced for bi-axial tension,[30–37] shear[38,39] and compression[20] of woven reinforcements (see Chapter 3). Based on the increasing power of computers,

these approaches aim to describe in detail the 3D behaviour of the fabric constituents including contact and friction and to obtain result fields at a local level.

Finite element modelling encounters two difficulties. First, the geometry of a textile unit cell is very complex, and creating a solid model manually is not an easy task. The solution is provided by the use of a textile geometry modeller as a preprocessor, capable of creating a finite element model automatically.[40–48] Second, the description of the material behaviour used in the finite element model must realistically represent the actual behaviour of the fibrous assemblies – yarns. Development of such a library of material models for textiles, available in finite element packages, presents a serious challenge to researchers.

Models of textile deformability developed so far have built a solid foundation for their generalisation, encapsulating the achievements of textile material science in a modelling software tool, allowing wide variability of textile structure and yarn parameters, instrumented with visualisation features and able to transfer the models of textile geometry into specialised micro-mechanical and flow modelling software as well as into general purpose finite element packages. Such a tool can be considered as a preprocessor for calculation of homogenised properties – permeability tensor and stiffness matrix – of deformed textile reinforcement. These properties, in their turn, are used as input to provide local parameters in modelling of Darcy flow through the deformed preform and structural finite element analysis of a 3D shaped composite part. This work is in progress in Composite Materials Group in the Department MTM, K.U. Leuven.[21,49–57] It has resulted in the development of textile modelling software *WiseTex* (http://www.mtm.kuleuven.be/Research/C2/poly/software.html). The chapter describes models of deformability of woven fabrics implemented in *WiseTex*. First versions of the models described here were developed in the early 1990s.[58–63]

4.2 Mechanical model of the internal geometry of the relaxed state of a woven fabric

The comprehensive description of the model of the relaxed state of a woven fabric can be found elsewhere.[49,51,53,64] Here we state its main components used in the simulation of the fabric deformation.

4.2.1 Weave pattern and elementary crimp intervals

A weave pattern (for one- and multilayered fabrics) is coded with matrix coding.[21,49,51,53] It allows separation of the crimped shape of the warp and weft yarns into elementary bent intervals (Fig. 4.1), representing sections of the yarn between interlacing sites. The shape of the yarn on an elementary interval is described using a parameterised function $z(x; h/p)$, where z and x are coordinates of the yarn middle line, h is the crimp height and p is the distance

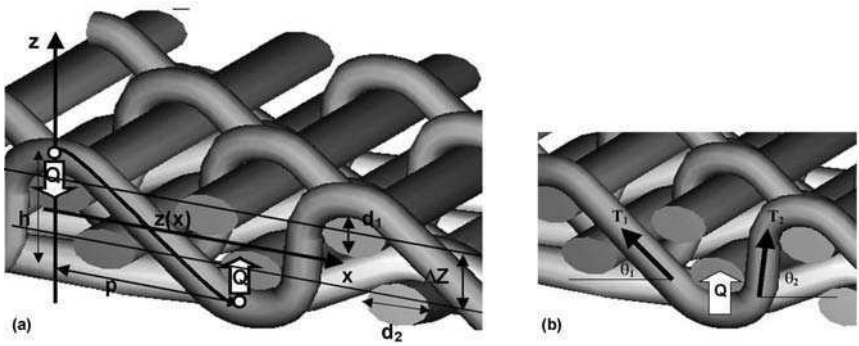

4.1 Model of internal geometry (a) and tension (b) of woven fabric.

between the interval ends (spacing of the yarns). The shape $z(x;h/p)$ for a given relative crimp height h/p is computed using the principle of minimum bending energy of the yarn on the interval and has the form:

$$z(x)h[1/2 - 3(x/p)^2 + 4(x/p)^3 + A(h/p)(x/p)^2((x/p) - 1)^2((x/p) - 1/2)] \quad 4.1$$

where the first term is a spline function, corresponding to the solution of the linearised minimum energy problem, and the second term represents a correction for a non-linear formulation. The function $A(h/p)$ is calculated from the solution of the minimum energy problem and is tabulated.

With this function known, the *characteristic function F* of the crimp interval is computed, representing the bending energy of the yarn:

$$w = \frac{1}{2}\int_0^p B(\kappa)\frac{(z'')^2}{(1+(z')^2)^{5/2}}\mathrm{d}x = \frac{B(\bar{\kappa})}{p}F(h/p) \quad 4.2$$

where $B(\kappa)$ is the (measured experimentally) bending rigidity of the yarn, which depends (non-lineary) on the local curvature $\kappa(x)$, or, after the integration, on an average curvature over the interval

$$\bar{\kappa} = \sqrt{\frac{1}{p}\int_0^p \frac{(z'')^2}{(1+(z')^2)^{5/2}}\mathrm{d}x} \quad 4.3$$

Function $F(h/p)$ is also tabulated. With the function F known, the transversal forces acting on the interval ends can be estimated as

$$Q = \frac{2w}{h} = \frac{2B(\bar{\kappa})}{p^2}\frac{p}{h}F(h/p) \quad 4.4$$

4.2.2 Compression of the yarns in the relaxed fabric

Warp and weft yarns in the relaxed fabric are compressed by the transversal forces Q [4.4] according to experimental diagrams, measured on 'virgin' yarns

$$d_1 = d_{10}\eta_1(Q), \quad d_2 = d_{20}\eta_2(Q) \tag{4.5}$$

where subscript '0' refers to the uncompressed state of the yarn, d_1 and d_2 are dimensions of the yarn cross-section (Fig. 4.1). These dimensions and crimp heights of the yarns are interconnected:

$$h^{Wa} = \Delta Z + (d^{Wa} + d^{We}) - (h_1^{Wa} + h_2^{We})/2 \tag{4.6}$$

where superscripts refer to the warp and weft yarns, subscripts '1' and '2' refer to two weft yarns in different layers, ΔZ is the distance between fabric layers (Fig. 4.1).

With crimp heights of weft yarns given, equations [4.4–4.6] provide a closed system of non-linear equations for calculation of the transversal forces Q and yarn dimensions d_1 and d_2.

4.2.3 Minimum energy problem – calculation of the weft crimp heights

The weft crimp heights are found using the principle of minimum bending energy of the yarns inside the unit cell. It is written as

$$W_\Sigma = \sum_{i=1}^{N_{Wa}} \sum_{k=1}^{K_i^{Wa}} w_{ik}^{Wa} + \sum_{j=1}^{N_{We}} \sum_{k=1}^{K_j^{We}} w_{jk}^{We} \rightarrow \min \tag{4.7}$$

where subscripts i, j refer to different warp and weft yarns, k to the elementary crimp interval of the warp/weft yarn, and energies of the elementary intervals are calculated using (2). The minimum problem [4.7] is solved for the weft crimp heights, with all other parameters defined inside the minimisation algorithm obtained via solution of the system [4.4–4.6] for the given current crimp heights. It takes about 1 s on 1 GHz PC to compute parameters for a 3D fabric with 20 yarns in the repeat, and about 0.05 s – for a plain weave fabric.

4.3 Model of compression of woven fabric

4.3.1 Outline of the algorithm

When a fabric is compressed, the following changes in geometry take place:

- warp and weft yarns are compressed;
- the less crimped yarn system increases its crimp, and the more crimped system reduces in crimp.

These two processes are treated in the model separately. This follows from the assumption of an even distribution of the compressive force over warp/weft intersections, because this assumption implies that force per intersection, which compresses the yarn cross-sections and bends the yarns, is independent of any changes of warp and weft crimp or cross-section dimensions.

To compute compression of the yarns, the compression force per intersection is evaluated:

$$Q_c = F/(N_{Wa}N_{We}) \tag{4.8}$$

where F is the pressure force on fabric repeat. This value is added to all the Q_{ij} – transversal forces acting on the intersections and computed with [4.4], to evaluate the dimensions of the yarns with [4.5]. Hence, both the compression due to yarn bending and the compression due to external force are accounted for. The algorithm presented above is then applied to yield the compressed dimensions of the yarn cross-sections and the new values of the yarn crimp.

The change of crimp in compression (increasing for warp and decreasing for weft, or vice versa) leads to a decrease of the fabric thickness. Therefore the basic mechanical equation governing this process is

$$\begin{aligned}&\text{work of compressive force } Q \text{ on change of thickness } db\\ &\quad = \text{change of bending energy of yarns } dW\end{aligned} \tag{4.9}$$

The compression of yarns has been accounted for before and the resulting changed cross-section dimensions are 'frozen', that is why the work of yarn compression does not enter the balance [4.9].

Changes of the fabric thickness db and bending energy of the yarns dW depend on the change of the *set* of weft crimp heights $\{dh_j^{We}\}$ and therefore [4.9] has a *set* of unknown variables. A reasonable assumption to cope with this difficulty is: 'The crimp changes in such a way as to provide the maximum possible change of thickness'. This means that if the function $b(\{h_j^{We}\})$ is considered (b being the fabric thickness), then changes of crimp will follow the direction of the maximum slope (in the opposite direction):

$$\{dh'_{ij}\} = -x\ grad\ b(\{h_j^{We}\})$$

where x is computed to satisfy [4.9]; dashed values refer to changed crimp. Equation [4.9] is then written as follows:

$$\begin{aligned}F \cdot \lfloor b(\{h_j^{We}\}) - b(\{h_j'^{We}\})\rfloor &= \sum_{i,k} W^{Wa}(\{h_j'^{We}\}) + \sum_{j,k} W^{We}(\{h_j'^{We}\})\\ &\quad - \sum_{i,k} W^{Wa}(\{h_j^{We}\}) - \sum_{j,k} W^{We}(\{h_j^{We}\})\end{aligned} \tag{4.10a}$$

$$h_j'^{We} = h_j^{We} - x \cdot grad\ b(\{h_j^{We}\}) \tag{4.10b}$$

to be solved numerically for x, which should also satisfy

$$0 \le h_j^{We} \le h_j^{We,max} \quad \text{and} \quad b(\{h_j^{We}\}) - b(\{h_j'^{We}\}) \ge 0 \tag{4.11}$$

4.3.2 Compression of 2D laminates

Woven preforms are usually compressed in a mould as a stack of fabric layers, which are not precisely positioned one against another, causing a geometric and mechanical phenomenon of *nesting*. Nesting plays an important role in determining the permeability of the laminate and the mechanical properties of the composite. Nesting causes a statistical distribution of the laminate properties, both at different positions within a composite sample and between different samples in a set of otherwise identical parts.

To calculate compression of a laminate, consider first compression of one layer of the fabric. After the calculation described above, the dimensions and placement of the yarns inside the unit cell of compressed fabric are known. The placement hence defines the *surface profile functions* of the face and back surface of the laminate (Fig. 4.2a):

$$\begin{aligned} h_f(x,y) &= \frac{Z}{2} - z_f(x,y) \\ h_b(x,y) &= z_b(x,y) + \frac{Z}{2} \end{aligned} \qquad 4.12$$

where x, y, z are Cartesian coordinates, with the centre of the coordinate system in the centre of the unit cell, Z is the fabric thickness, z_f and z_b are coordinates of the face and back surface of the fabric. Equation [4.12] applies if there is a point (x,y,z) inside the yarns or fibrous plies for the given (x,y). If no such point exists, then

$$h_f(x,y) = h_b(x,y) = Z$$

With the surface profile functions defined, it is easy to calculate the nesting of the layers. Consider two identical layers of the laminate, with one layer shifted relative to another by dx and dy in x and y directions (Fig. 4.2b). To define the nested position, we must calculate the distance h^* between centre planes of the layers, when the yarns in the layers are just touching one another and there is no inter-penetration of the yarns. When nesting is zero, $h^* = Z$. Consider a certain distance between centre planes h. The distance (depending on the (x,y) position) between the back surface of the upper layer and the face surface of the lower layer is

$$\delta(x,y;h) = h - Z + h_f(x,y) + h_b(x - dx, y - dy)$$

Defining

$$\delta^*(h) = \min_{x,y} \ \delta(x,y;h)$$

we can compute the nesting distance h^* as a solution of the equation

$$\delta^*(h) = 0$$

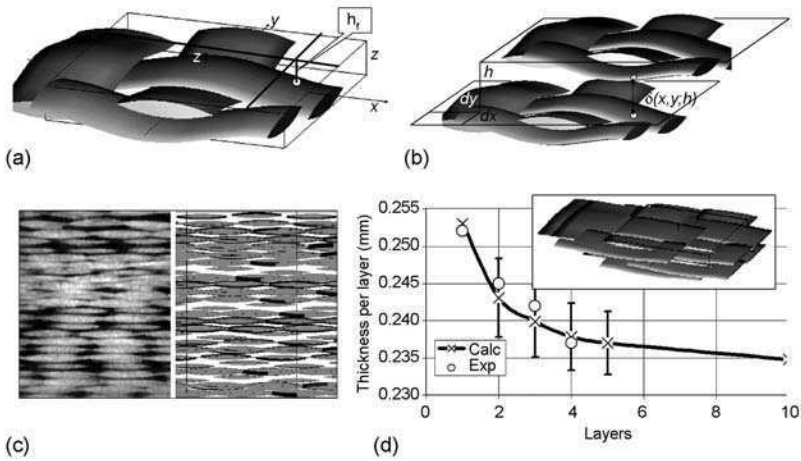

4.2 Nesting model: (a) Surface depth function h_f; (b) Shifted layers; (c) Captured with X-ray microCT and computed cross-section of 25 ply laminate; (d) thickness of laminate per layer vs number of layers.

If the surface depth functions are defined on a finite mesh, these calculations are easily performed if shifts *dx, dy* are done in integer mesh units. In this case the calculations involve $O(Nx * Ny)$ comparisons, *Nx* and *Ny* being the mesh size in *x* and *y* directions.

For a laminate of *L* layers, the set of shifts dx_l, dy_l, $l = 1 \ldots L$ is defined, and the algorithm is applied to one layer after another. When the nested positions of layers are defined, the descriptions of the yarns and fibrous plies of the original one-layer fabric are copied and positioned according to the in-plane shifts and vertical placement of the layers (Fig. 4.2c). Note that the configuration shown in Fig. 4.2 is subject to the translational symmetry transformation in the *x–y* plane, and the apparent voids in the unit cell volume are actually filled by the yarns belonging to the adjacent repeatable units.

Figure 4.2c compares the simulations with experiment for a glass fabric with 3.34 warp yarns/cm and 3.62 weft yarns/cm, 600 tex yarns, areal density 420 g/m^2. The compressibility of the fabric has been studied by Lomov and Verpoest,[21] where the precision of the *WiseTex* compression model has been validated. Consider laminates made of this fabric under a pressure of 1 MPa. Comparison between an experimental cross-section of the laminate and a result of the random simulation (Fig. 4.2c) reveals similarity between the qualitative characteristics of the placement of the layers. In both cases, there exist regions with high packing density of the yarns, where the local fibre volume fraction is very high, and regions with high porosity, effectively creating channels in the fabric. Figure 4.2c shows also the experimental data on the thickness of the laminate with one, two, three and four layers,[21] in comparison with the results of Monte-Carlo simulations of the random

stacking of the fabric layers (size of the sampling 500). The experimental and computed data correspond quite well.

4.3.3 Compression of 3D fabric

The algorithm described above does not preserve the length of the yarns after compression, hence introducing an error on the final fabric geometry. In the compaction of a 2D fabric this error is small and can be considered to be negligible. When a 3D fabric is compacted, its z-yarns (going through the thickness), deviate considerably from their paths, as the length of the yarn must be preserved when the thickness of the fabric is reduced. In a 3D fabric with z-yarns initially almost vertical, they will acquire S/Z shapes. If the interlacing yarns are oblique, their initial slope is increased.

To describe such behaviour rigorously, one would have to account for all kinds of contacts between yarns occurring during the compaction. This task may be an interesting challenge for finite element modelling. In the present model, implemented in *WiseTex*, a simple geometrical approach is followed. A spline correction is added to the yarn path, with spline coefficients chosen as to preserve the yarn length after the deformation. The result of the correction is illustrated in Fig. 4.3, which shows the results of measurement and simulation of compression of 3D glass fabric (yarns $4 \times 4 \times 33$ tex, 35 yarns/cm in warp and weft, areal density 3900 g/m^2, weave is shown in the figure). The fabric is proposed in Parnas *et al.*[65] as a benchmarking case for study of RTM composite processing. Compression of the fabric has been measured on the KES-F (Kawabata Evaluation System) textile compression tester for the low load range and on an Instron for higher loads. The input data on compressibility of the yarns and their bending rigidity has been measured on KES-F. Other fabric data was

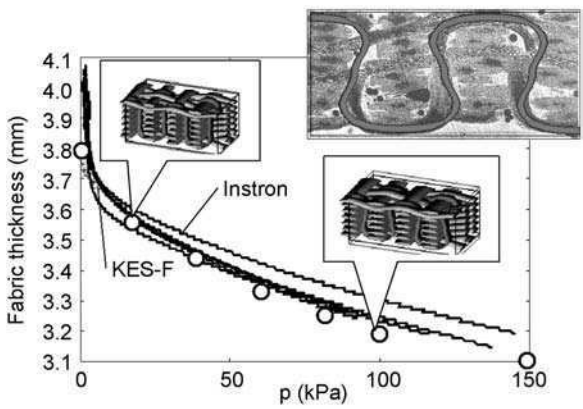

4.3 Compression of 3D fabric. Above: Compression diagram, measured (lines) and computed (circle). Inset: Computed and observed shape of z-yarn at 300 kPa.

taken as specified in Parnas *et al.*[65] We see that the described algorithm provides a reasonable prediction of the compression diagram as well as the fabric internal structure after compression.

4.4 Model of uniaxial and biaxial tension of woven fabric

4.4.1 Outline of the algorithm

The algorithm described here is a generalisation of the method, proposed by Kawabata *et al.*[3,4] and Olofsson[66] and widely used by other researchers for plain weave fabrics (with possible extension to other 2D structures).[15] The computational scheme was also implemented into FEA.[30,31] We apply the method to a generalised description of an arbitrary weave, including 3D architectures.

Consider first a woven fabric under biaxial tension characterised by deformations in warp (x-axis) and weft (y-axis) directions $e_x = Y/Y_0 - 1$, $e_y = X/X_0 - 1$, where X and Y are sizes of the fabric repeat, subscript '0' designates the undeformed state. As discussed above, the internal structure of the fabric is described based on weft crimp heights h_j^{We} and weft and warp cross-section dimensions at the intersections d_{ij}^{Wa} and d_{ji}^{We} (subscripts designate different yarns in the fabric repeat). These values change after the deformation. Tension of the yarns induces transversal forces, which compress the yarns, changing the d values. The same transversal forces change the equilibrium conditions between warp and weft, which leads to a redistribution of crimp and change of crimp heights. When the mentioned values in the deformed configuration are computed, the internal geometry of the deformed fabric is built as explained above. Change of length of the yarns determines their average (in the repeat) deformations, which, through the tension-deformation diagrams of the yarns allow yarn tensions to be computed. When summed, with yarn inclinations due to the crimp accounted for, the yarn tensions are transformed into loads, causing the fabric deformations.

The key problem in biaxial modelling is the computation of the crimp heights and transversal forces in the deformed structure. Assuming that the spacing of the yarns in the fabric is changed proportionally to the change of the repeat size, we compute the x and y positions of intersections of warp and weft in the deformed structure. The configuration of the yarns in the crimp intervals between the intersections is determined by these positions and (unknown) crimp heights. Consider some values of the crimp heights. Then the geometrical model determines the positions of the ends of crimp intervals (warp/weft intersections) and bent shape of the yarns in the intervals.

The transversal forces are computed using the following formula (Fig. 4.1b):

$$Q = Q_{bend} + T_1 \sin\theta_1 + T_2 \sin\theta_2 \qquad 4.13$$

where Q_{bend} is the transversal force due to yarn bending [4.4], $T_{1,2}$ are the yarn tensions on two crimp intervals adjacent to the point of application of the transversal force, $\theta_{1,2}$ are the angles of inclination of the yarn on these crimp intervals. We assume that the tension of the yarn can be computed based on the average deformation ε of the yarns (therefore $T_1 = T_2$):

$$T_1 = T_2 = T(\epsilon); \epsilon = \frac{l - l_0}{l_0} \qquad 4.14$$

where l is the yarn length. Note that T depends on yarn length after the deformation, which in its turn depends on crimp heights and yarn dimensions.

The transversal forces compress the yarns according to an experimental compression law [4.5]. When the yarn dimensions are computed and 'frozen', crimp heights are determined using the minimum energy condition:

$$W = W_{bend} + W_{tens} \rightarrow \min$$

where W_{bend} and W_{tens} are the bending and tension energy of the yarns. The former is computed summing up bending energies of the yarns in crimp intervals between yarn intersections [4.7], the latter is the sum of tension energies of all the yarns, which are computed using their (linear or non-linear) tension diagrams and yarn deformations.

The computations described above determine one step in the iteration process: starting from current values of the crimp heights we compute yarn lengths, yarn tensions, transversal forces, yarn compressed dimensions and then new values of the crimp heights. The full algorithm is depicted in Fig. 4.4.

If one side of the fabric is kept free (uni-axial tension, say, along the warp), then the described algorithm has another, outer iteration loop, searching for $X < X_0$ (negative e_y) which would lead to zero loads along the weft (y) direction. This allows computing the Poisson coefficient for the fabric.

4.4.2 Comparison with finite element simulation and experiment

Experimental biaxial tensile properties of balanced glass woven fabric (plain weave, 2.2 yarns/cm, 1220 tex) and results of finite element (FE) analysis have been reported in refs 32, 33 and 55. The main feature of FE calculations is the specific mechanical behaviour of the single yarn, which is composed of thousands of fibres with very small sections, which are very flexible and can slide relative to others. The behaviour of the yarn is assumed to be orthotropic. Shear moduli are very small. Young's moduli in the direction perpendicular to the yarn are all very small in comparison to the modulus in the direction of the yarn. A hypoelastic orthotropic model is used and the rotation of the orthotropic frame (as well as the rotational objective derivative) is based on the rotation of the yarn. The compression of the yarn is very important in biaxial tension,

Step 1. Set initial deformations and tensions.
Step 2. Compute dimensions of yarns and transversal forces.
Step 3. Compute length of the yarns.
Step 4. Compute deformations and tensions.
Step 5. Check convergence for the deformations. If not, go to *Step 2*.

Step 1. Set an approximation $\{h_{lj}^{We}\}$.
Step 2. Compute $grad(W\{h_{lj}^{We}\})$.
Step 3. Solve the minimization problem in the gradient direction.
Step 4. Check the convergence of $\{h_{lj}^{We}\}$; if not, go to *Step 2*.

Step 1. Compute spacing $p_{Wa0}(1+\epsilon_y)$; $p_{We} = p_{We0}(1+\epsilon_x)$.
Step 2. Set changes of weft crimp heights $\Delta h_{lj} = 0$.
Step 3. Compute fabric **internal structure** for $h_{lj} = h_{lj0} + \Delta h_{lj}$.
Step 4. Compute average **yarns strains** $\epsilon = l/l_0 - 1$.
Step 5. Compute yarns tensions $F = F(\epsilon)$.
Step 6. Compute **transversal forces** Q (due to bending and tension).
Step 7. Compute **compression** of the yarns under the forces Q. Check convergence of Q.
Step 8. Compute Δh_{ij} using the condition of **minimum of total (bending plus tension) energy** of the yarns in the repeat.
Step 9. Check convergence of Δh_{lj}; if not, go to *Step 3*.
Step 10. Compute applied forces summing up the yarns' tensions.

4.4 Biaxial tension algorithm.

because the undulation variations directly depend on these thickness changes. The transverse Young's modulus is assumed to be of the form.

$$E_3 = E_\epsilon + E_0|\epsilon_{33}^n|\epsilon_{11}^m \qquad 4.15$$

E_ϵ is the transverse Young's modulus of the unloaded state. It is very weak (nearly equal to zero) for the single yarns of the studied fabrics. The parameters E_0, m, n are determined using an inverse method from the biaxial test for equal forces in the warp and weft direction (Fig. 4.5a). The results of the finite element analysis are in good agreement with the experimental data.[32–34]

The current formulation of the approximate model (Fig. 4.4) does not envisage the dependency of the yarn compression diagrams on the applied tension. Therefore comparison of the experimental data and results of finite element simulations can answer two questions:

- Does the iterative algorithm of Fig. 4.4, simplified vis-à-vis finite element modelling, provide results close to the latter (and to experiment)?
- What are the errors introduced by using compression diagrams obtained without the yarn tension?

To answer these questions, *WiseTex* modelling of the tension of the fabrics, described above, have been performed. The yarn tension resistance has been taken from the experiment (Fig. 4.5). Bending rigidity of the yarns has been

measured on KES-F to provide the value of 0.5 Nmm^2. The compression law was derived from equation [4.15] using different constant levels of tension (ϵ_1). These diagrams are referred as 'Compression $\epsilon_1 = \ldots\,\%$'.

Figure 4.5 shows the results. The calculations describe well the qualitative difference between deformation regimes of uniaxial and biaxial tension. For the uniaxial tension the error of calculations is small whatever compression diagram is used. The standard textile compression tester can be used to gather input data for simulation of this tension regime. For the biaxial tension the difference between calculations with compression laws corresponding to different tensions can be as large as 30%. A reasonable correlation is found when the compression

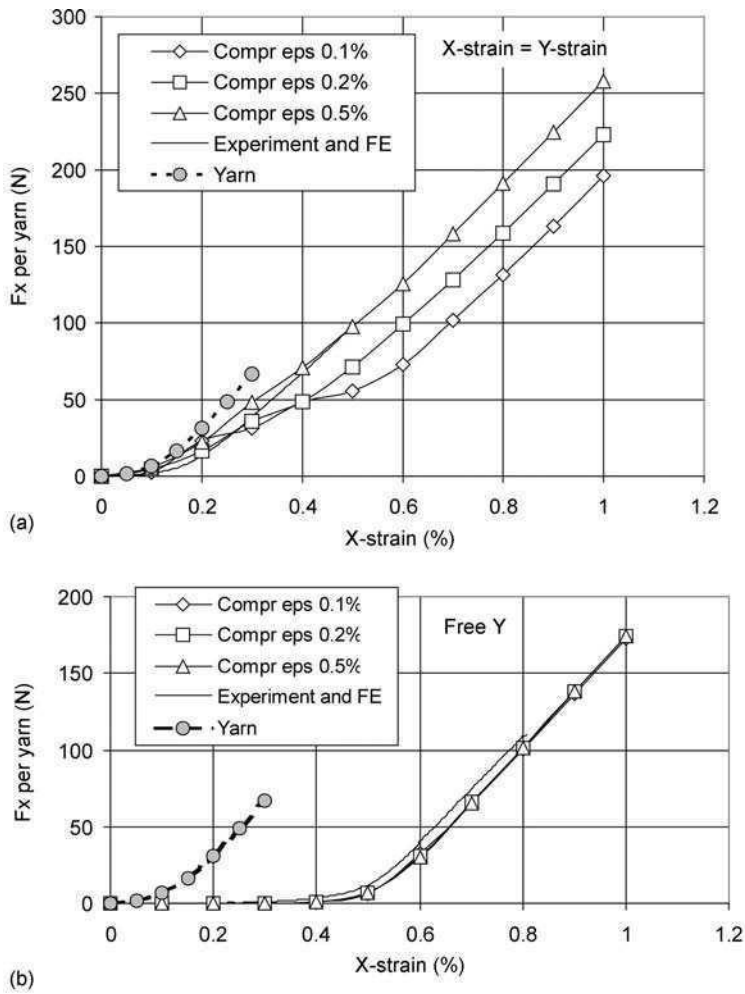

4.5 Computed and measured tension force: (a) biaxial (equal forces in warp and weft direction) and (b) uniaxial tension.

diagram used corresponds to the highest level of strain of the yarns. For the low strain region the experimental curve corresponds better to the calculations with compression diagrams for low tension, and vice versa for higher strain.

4.5 Model of shear of woven fabric

In formulating the model we again follow the approach outlined by S. Kawabata in the 1970s,[5] which is also used in more recent publications.[22–25,67,68]

Our aim is, given a value of the shear angle, γ, to compute the shear force, T, in the presence of (pre)tension of the fabric. The tension is dealt with according to the algorithms of the previous section, resulting in values of the tension of yarns and transversal forces Q, associated with it [4.13]. Therefore we introduce an important assumption: tension of the yarns and transversal forces are computed for the non-sheared configuration and do not change during the shear deformation. This may lead to errors of two types:

- Neglecting the forces in the direction of the yarns, developed during shear. Using general equations, describing the plane stress-strain state of an equivalent continuous membrane, these forces can be calculated as $F^* = T \sin 2\gamma$. With pretension force in the order of 1 N/mm, and shear forces of 0.010.1 N/mm (see the examples in Section 4.6.3 below), the corresponding error is a few percent.
- Change of the yarn tension due to the change of the angle of intersection of the yarns, yarn dimensions, crimp heights during shear. These factors could affect yarn tension (for the same overall deformation of the fabric in the direction of the yarns) also by only a few percent.

Introducing an appropriate calculation loop could eliminate both errors. This complication of the algorithms has not been deemed necessary, as overall precision of the calculation of the shear force, connected with uncertainties of the input data, is also not better than 10 to 20%.

Consider a sheared unit cell of a woven fabric (Fig. 4.6). For simplicity the illustrations below show a plain weave unit cell. The equations are, however, applied to elementary crimp intervals and the forces are summed for the actual fabric repeat. An account is taken therefore of the differences imposed by the weave pattern, as shown in comparison with experimental data below.

Consider a change of shear angle $\Delta\gamma$. The mechanical work ΔA of the shear deformation is (Fig. 4.6):

$$\Delta A = TXY \cos\gamma \Delta\gamma \qquad 4.16$$

where X and Y are the dimensions of the unit cell; units of T are N/mm, corresponding to the 2D nature ('membrane') of the problem. Usage of shear force per unit length also has been proven experimentally to be a correct normalisation procedure for the picture frame test.[69] We will take into account the following mechanisms of the yarns deformation, determining the shear

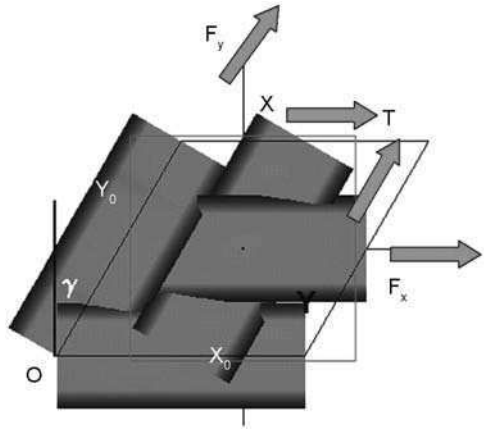

4.6 Sheared unit cell of woven fabric.

resistance: friction; (un)bending; lateral compression; torsion; vertical displacement. Accordingly the mechanical work A is subdivided:

$$\Delta A = \Delta A_{friction} + \Delta A_{disp} + \Delta A_{bending} + \Delta A_{torsion} \qquad 4.17$$

The lateral compression of the yarns is introduced via the transversal forces. We do not consider intra-yarn friction here, as suggested in ref. 70. It is felt that this factor is accounted for by the lateral compression calculations, but the question needs more careful examination in future work, especially in the light of experimental evidence of intra-yarn shear.[71]

The transversal forces, acting on the yarns and determining the friction between them, are caused by tension and bending of the yarns [4.13]. During the shear, yarns are subject to the lateral compression, which creates a pressure inside yarns, which results in an additional component of the transversal force acting on the yarns of the interlacing system. Therefore the transversal forces at yarn intersections will be

$$Q = Q_{bending} + Q_{tension} + Q_{compression} \qquad 4.18$$

where the first two terms are computed with [4.4] and [4.13]. The last term is calculated by the change of fibre volume fraction inside the yarn (Fig. 4.7a) and experimental compression diagram of the yarn:

$$Q_{compression} = (P_{Wa} + P_{We}) \cdot d_{Wa2} d_{We2}$$

where P_{Wa} and P_{We} are pressures inside warp and weft yarn, calculated as

$$P = P(Vf(d_1, d_2))$$

where the fibre volume fraction Vf is inversely proportional to the area of the compressed cross-section with dimensions d_1 and d_2, and the dependency $P(Vf)$ is measured in the compression experiment.

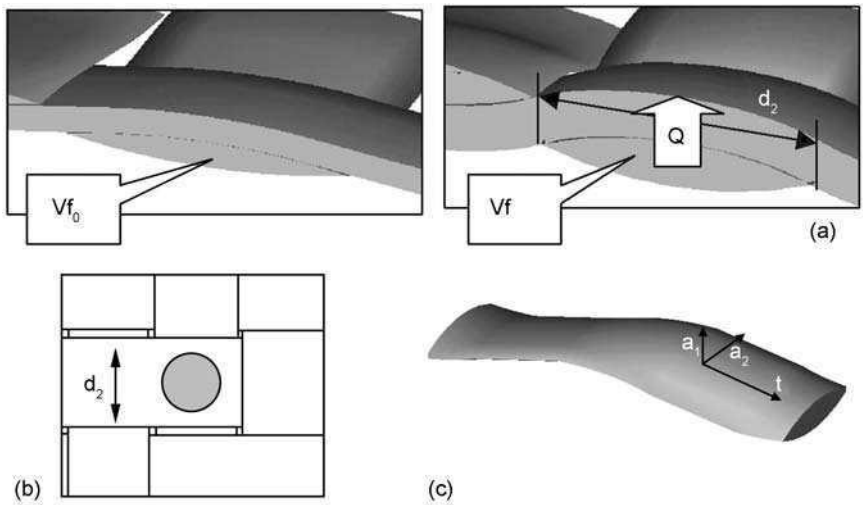

4.7 Components of shear resistance: (a) lateral compression; (b) friction; (c) torsion.

The components of the shear resistance are computed as follows.

Friction moment (Fig. 4.7b)

$$M_{friction} = fQr; \quad r = \frac{2R}{3}; \quad R = \tfrac{1}{2}\sqrt{d_{Wa2}d_{We2}} \qquad 4.19$$

$$\Delta A_{friction} = M_{friction}\Delta\gamma$$

where f is the coefficient of friction, r is the effective radius of the zone of friction for the normal force Q evenly distributed over a circle with radius R, d_2 is the width of the intersecting warp and weft yarns.

The definition of R is an assumption, valid for flat, low crimp rovings, when the contact zone of the yarns can be expected to cover all the yarn width. Leaf and Sheta[72] use a correction accounting for a possible lesser contact zone for more rounded yarns. The accurate definition of the contact zone is out of scope of the present model, hence introduction of the correction does not seem to be justified. Note that assumption of wide contact [4.19] may lead to over-estimation of $M_{friction}$, whilst neglect of the curvature of the contacting surfaces (more important for less flat yarns) leads to underestimation of it. Comparisons[73] of estimations by [4.19] with direct measurements of the friction moment between two intersecting yarns by Kawabata,[5] place the experimental values within the range of the predictions, given uncertainties in the friction coefficient values, and do not show systematic errors of equations [4.19].

Mechanical work of torsion (Fig. 4.7c)

$$\Delta A_{torsion} = C\tau\Delta\tau; \tau = \int_0^s \mathbf{t} \cdot \left(a \times \frac{d\mathbf{a}}{ds}\right) ds$$

where C is the torsional rigidity of the yarn, τ is the full angle of torsion, computed by integration of rotation of vector $\boldsymbol{a}$, determining orientations of the yarn cross-section axis, about the tangent to the yarn middle line $\boldsymbol{t}$, over the yarn length. Measurement of the torsional rigidity of yarns requires non-standardised equipment,[74] which is normally not suitable for heavy yarns used in composite reinforcements. It the absence of direct measurement, it can be estimated as $C = B/(d_2/2)$, where B is the bending rigidity of the yarn, and d_2 its width.[75]

Mechanical work of (un)bending of the yarns

$$\Delta A_{bending} = \frac{1}{2} B \int_0^S \left(\frac{d^2\delta z}{ds^2}\right)^2 ds$$

where δz is the difference between the z-coordinate of the centre line of the yarn before and after the deformation (at a given coordinate along the yarn s).

Mechanical work of vertical displacement of the yarns (this displacement goes against the transversal forces Q)

$$\Delta A_{disp} = Q \cdot \frac{1}{l} \int_{contact} \delta z \cdot ds$$

where l is the yarn length, and the integration is performed over the contact zones between warp and weft yarns, determined by the geometrical model.[51,76]

With the components of mechanical work [4.16] known, equation [4.15] is integrated to yield the dependency $T(\gamma)$. Note that the result of the calculation depends on the applied tension (via $Q_{tension}$). This dependency and comparison of the model with experiment is discussed in detail in the next section.

4.6 Parametric description of fabric behaviour under simultaneous shear and tension

Using the model outlined above, a designer can get input data for forming simulations. However, getting input data for the model is also difficult, as this involves testing of the yarns on specialised textile testing equipment. For some classes of reinforcement materials it is possible to make a generic characterisation of them, depending on a few parameters, and then, using the theoretical model, produce analytical expressions for shear behaviour.

4.6.1 Properties of glass rovings

Woven glass fabrics are a common reinforcement for composite materials. The raw materials, glass rovings, are produced by different manufacturers (terms *rovings, yarns* and *tows* are used below as synonyms). The results shown here[21,55,77] cover the full range of linear density from 150 to 5000 tex. All the measurements were done on 'virgin' (before weaving) rovings.

Width and thickness

The width of a roving was measured at 20 points along the yarn length on the scanned (1200 dpi) images of rovings lying flat. The thickness of a roving was determined by the extrapolation of the compression curve (see below) to zero pressure. Measurements of the thickness with a calliper or a textile thickness meter is done under a certain pressure (uncontrollable in the former and controlled in the latter case) and therefore does not provide correct values for a free yarn. Figure 4.8a,b shows a summary of the results. The data are reasonably approximated by a linear dependency of the roving width and thickness on the linear density.

Bending

Bending of rovings was also measured on KES-F. Single yarns were tested. In the first stage of bending, the fibres tend to buckle, breaking the sizing and resulting in a sharp increase of stiffness.[21] Therefore the first loading cycle was discarded from data processing. Sometimes the same phenomena occur when reversing the direction of bending. In these cases the corresponding loading part of the curve was also discarded. For each type of yarn three samples were tested; for each sample three full bending cycles were performed and the second cycle was used in the data processing using the standard KES-F routine: bending rigidity is determined by the slope of the diagram between curvatures of 0.5 and 1.5 cm^{-1}. Figure 4.8c shows dependency of the bending rigidity on the linear density of the yarns. The tested rovings have fibres of different diameter d (from 16 to 21 m). The scatter of 30% in the diameter gives a scatter of 300% in the bending rigidity of the fibres (proportional to d^4) and 70% in the bending rigidity of fibre bundles with the same linear density, but with fibres of the different diameter (proportional to d^2 for the case of non-interacting fibres). This explains the significant deviation of some data points from the average 'master' curve for yarns with linear density less then 1000 tex. However, the general agreement of the quadratic approximation of the 'master' curve with the data is sufficiently high.

Compression

Compression of rovings was measured on KES-F apparatus, following the routine prescribed by the KES-F manual. The maximum force used was 100 cN,

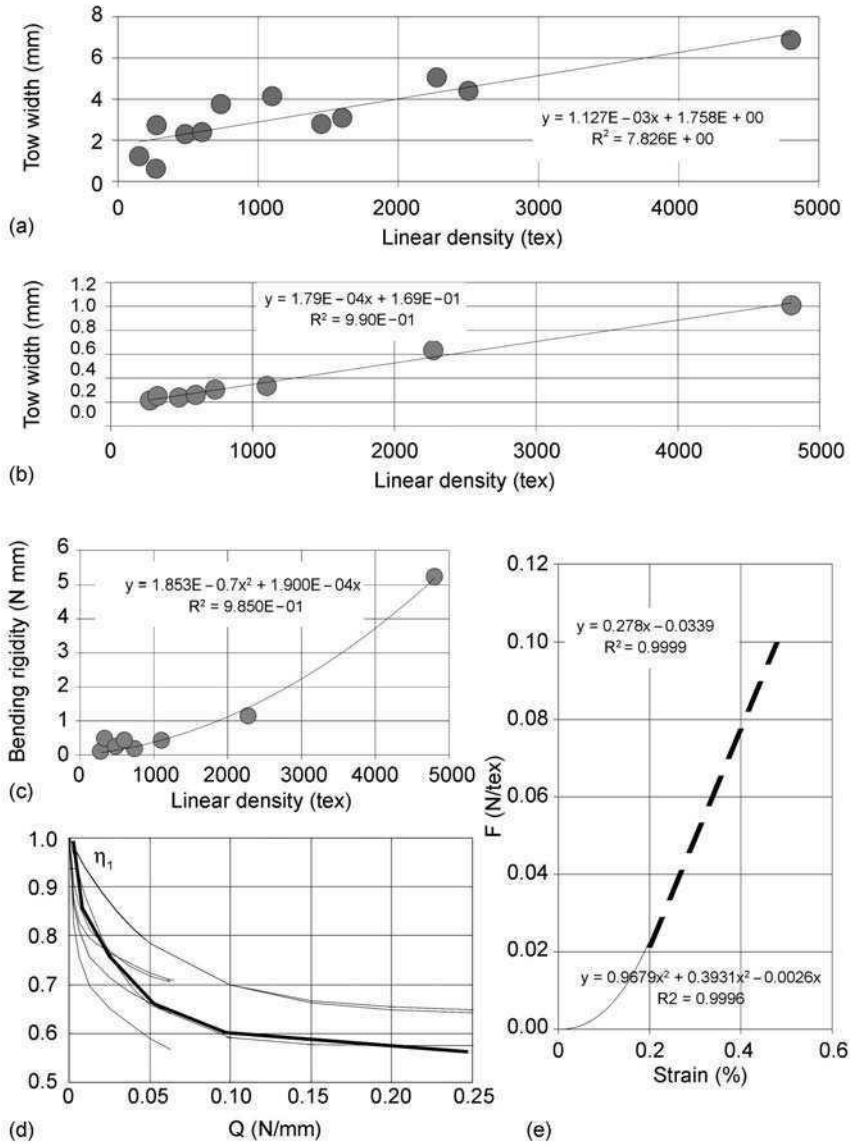

4.8 Properties of glass rovings: (a) width; (b) thickness; and (c) bending rigidity: points – measurements, line – linear/polynomial approximation; (d) compression diagram: thin lines – measurements for different rovings, thick line – least square approximation with [4.20]; (e) tension: solid line – non-linear, dashed line – linear region.

which corresponds to the compression force per unit length (4 mm under the machine's head) of 25 cN/mm. For the thicker rovings a larger head was used, which gives lower maximum force. For each type of yarn three samples were tested, with three compression cycles for each yarn. Following Lomov and Verpoest,[21] the second cycle of compression was used for final results.

For simulation of the compression behaviour of the yarns in the model the following data are needed: (1) dimensions of the yarn cross-section in free state d_{10} and d_{20} (thickness and width of the roving, see above); (2) functions $\eta_1 = \eta_1(Q)$, $\eta_2 = \eta_2(Q)$, $\eta_1 = d_1/d_{10}$; $\eta_2 = d_2/d_{20}$ [4.4]. The KES-F equipment does not provide data for the yarn flattening. Therefore an empirical relationship between η_1 and η_2 has been used:[73]

$$\eta_2 = 1/\eta_l^{0.33}.$$

The compression curves for the different rovings (Fig. 4.8d) demonstrate a significant scatter, without any recognisable trends relating to linear density or the tow thickness. The average 'master' diagram is built by the least square approximation by the formula

$$\eta_1 = \frac{1 + \left(\frac{Q}{Q_0}\right)^a \eta_{1min}}{1 + \left(\frac{Q}{Q_0}\right)^a}, \eta_{1min} = 0.5583, Q_0 = 0.0277, a = 1.7987 \quad 4.20$$

where Q_0, a and η_{1min} are the fitting parameters. The error of this approximation is about 15% ($R^2 = 0.76$).

Friction

The friction coefficient between roving and steel was measured on KES-F. The obtained value $f = 0.24$ was retained as the value for roving-roving friction, as it does not contradict with the literature data.[22]

Tension

Tension diagrams of the rovings were taken from the measurements in Boisse *et al.*[30] (Fig. 4.8e). We assume that the tension resistance of the rovings is proportional to the linear density. The tension diagram has two regions: non-linear, up to approximately 0.2% of strain and linear. The former represents straightening of the fibres in the tow. The tow resistance to tension is a combination of the (un) bending and tension resistance of the fibres. Proportionality of the tension force to the linear density of the tow is equivalent to the assumption that the waviness of the fibres is roughly the same in different rovings. The linear part of the diagram corresponds to tension of the straight fibres. The experimentally measured tensile modulus for this part of the diagram is slightly less than the tensile modulus of glass fibres 28.3 N/tex (72 GPa).

Summary of the 'master' descriptions of the properties of glass rovings

The result of the parametrisation of the properties of glass rovings is shown in Table 4.1. All the data necessary for the calculation of the shear diagram of a roving, are given as functions of the roving linear density.

4.6.2 Parameterisation of the shear diagram

A woven fabric is characterised by weave pattern, weaving density, and warp and weft yarn descriptions.

For the weave patterns, the three most widely used types were chosen for the numerical experiments: plain, twill 2/2 and satin 5/2. These patterns represent the range of the interaction intensity of the yarns in the weave: maximum possible for plain weave, average for twill 2/2 and weak for satin 5/2. One can expect a monotonic decrease of the shear resistance with weakening of the interaction of the yarns.

For the weaving density, only square (= identical warp and weft parameters) fabrics have been considered, being the most important practical case. Shear behaviour of non-balanced fabrics can be simulated using the same model, if needed. To characterise the weaving density, a *looseness factor s* has been introduced:

Table 4.1 Averaged dependencies of properties of glass rovings on their linear density *t*, tex

Property	Formula
Thickness d_1, mm	$d_1 = 1.79\text{E-}04 * t + 1.69\text{E-}01$
Width d_2, mm	$d_2 = 1.127\text{e-}03 * t + 1.758\text{E} + 00$
Coefficient of compression, η_1, as function of compressive force per roving length $[Q]$ = N/mm	$\eta_1 = \dfrac{d_1}{d_{10}} = \dfrac{1 + \left(\dfrac{Q}{Q_0}\right)^a \eta_{min}}{1 + \left(\dfrac{Q}{Q_0}\right)^a} = const\,(t),$
	$\eta_{min} = 0.5583, Q_0 = 0.0277, a = 1.7987$
Coefficient of flattening, η_2, as function of compressive force per roving length $[Q]$ = N/mm	$\eta_2(Q) = \dfrac{d_2}{d_{20}} = (\eta_1(Q))^{-0.33} = const\,(t)$
Bending rigidity B, N mm^2	$B = 1.85\text{e-}07 * t^2 + 1.90\text{E=}04 * t$
Coefficient of friction f	$f = 0.24$
Tension diagram 'force F vs strain ϵ', $[F]$ = N/tex, $[\epsilon]$ = %	$F = \begin{cases} 0.9679 \cdot \epsilon^3 + 0.3931 \cdot \epsilon^2 - 0.0026 \cdot \epsilon, & \epsilon \le 0.2\% \\ 0.278 \cdot \epsilon - 0.0339, & \epsilon > 0.2\% \end{cases}$

$$s = \frac{p - d_2}{d_2} \tag{4.21}$$

where p is the spacing of the yarns (inverse to the ends/picks count), d_2 is the yarn width. The looseness factor represents ratio of the width of the pores in the fabric to the yarn width. The range s = (0.01, 0.02, 0.05, 0.075, 0.1, 0.2, 0.5, 1.0) has been considered, where value $s = 0$ represents an extremely tight, and $s = 1$ an extremely loose fabric. The value of d_2 in [4.16] can be calculated for a given linear density of the yarns using the formula of Table 4.1.

Properties of glass rovings of a given linear density t are fully described by the formulae of Table 4.1. Hence t is the only parameter needed to characterise the warp and weft yarns (identical because of the assumption of square fabric construction). The range of t for the numerical experiments was t = (100, 200, 500, 1000, 2000, 5000) tex.

Finally, the shear resistance (shear diagram $T(\gamma)$) depends on the fabric (pre)tension. Only equal tension of the warp and weft has been considered (the case of non-symmetrical tension can be simulated with the same model if needed). The pretension is characterised by the tensile strain of the fabric $\epsilon = 0$ to 1%. The maximum value of 1% corresponds to the start of a considerable extension of the glass fibre (as opposed to the decrimping of the yarns)[30,55] and is not likely to be exceeded in the real forming processes.

The calculations followed the following steps for all combinations of parameters:

- For a given linear density of the yarns t, calculate yarn width d_1;
- Using a given looseness factor s, calculate spacing of the yarns p;
- Assign properties of the warp and weft yarns using the value of t and formulae of Table 4.1;
- Build a geometrical model of non-sheared fabric of a given weave pattern, calculated yarn spacing and calculated properties of the yarns;
- Apply the model of coupled biaxial tension and shear of the fabric for a given pretension of the warp and the weft and calculate the shear diagram $T(\gamma)$.

The numerical experiments resulted in a vast set of shear diagrams $T(\gamma; weave, t, s, \epsilon)$. The diagrams for the different weaves were further processed separately. The processing has been done in the following steps.

Shape of the shear diagrams

Consider a diagram $T(\gamma)$ for a given set of parameters (t, s, ϵ), a typical example of which is shown in Fig. 4.9. The diagram has been approximated with an analytical expression

$$T(\gamma) = T_0 + T_1 \tan^a \gamma \tag{4.22}$$

This formula [4.22] represents the main features of the shear behaviour:

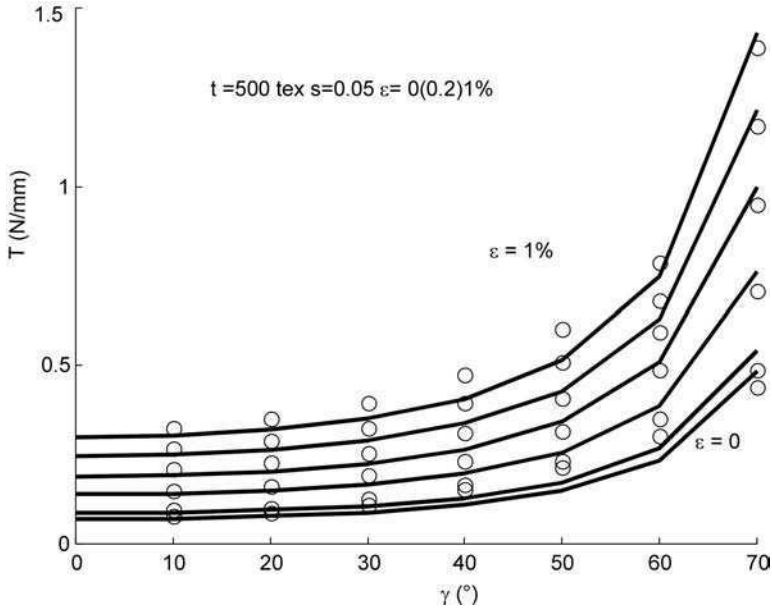

4.9 Simulated shear diagrams (points) and their approximation with equation [4.23] – lines. Plain weave, $t = 500\,\text{tex}$, $s = 0.05$, $\epsilon = 0(0.2)1\%$ (shear resistance monotonically increases with the increase of pre-strain s).

- Non-zero resistance from the very beginning of the shear ($\gamma = 0$), caused by the friction between the yarns
- Low shear modulus for low shear angles

$$G(\gamma) = \frac{dT}{d\gamma} = aT_1 \tan^{a-1}\gamma(1 + \tan^2\gamma) \underset{\gamma\to 0}{\longrightarrow} 0 \quad (a > 1)$$

- Locking behaviour for high shear:

$$T(\gamma) = \underset{\gamma\to\pi/2}{\longrightarrow} \infty, G(\gamma) \underset{\gamma\to\pi/2}{\longrightarrow} \infty$$

After fitting the calculated diagrams with [4.22], the value of a was found in all cases to lie inside the interval $(1 \ldots 3)$, without any clear trend in dependency on (t, s, ϵ). It was decided then to try to use the approximation [4.22] with $a = 2$ in all the cases. After refitting the data, the agreement between the approximation

$$T(\gamma) = T_0 + T_1 \tan^2\gamma \qquad 4.23$$

was found to be quite good. An example of the approximation is shown in Fig. 4.9. A certain systematic underestimation of the shear force by [4.19] in this figure is explained by the fact that it refers to a certain combination of the parameters t and s; for other combinations the constant value $a = 2$ leads to a certain overestimation.

The value $a = 2$ and analytical expression [4.23] were used in all the subsequent calculations. The coefficients in the equation [4.23] have a clear mechanical meaning: T_0 is the shear resistance at $\gamma \to 0$, caused by friction between the yarns, T_1 determines the shear modulus

$$G(\gamma) = \frac{dT}{d\gamma} = 2T_1 \tan\gamma(1 + \tan^2\gamma)$$

Coefficients T_0 and T_1

Coefficients of the formula [4.23] depend on parameters (t, s, ϵ). To establish these dependencies in a closed form, the calculated values of the coefficients were tabulated:

$$T_0 = T_0(t, s, \epsilon), \quad T_1 = T_1(t, s, \epsilon) \tag{4.24}$$

and a regression analysis was performed over the whole set of the data. After analysis of different representations of the regression formulae, the following equations were chosen to fit the data:

$$\ln T_0 = b_1 + b_2 \cdot \ln t + b_3 \cdot \ln s + b_4 \cdot \ln\epsilon + b_5 \cdot (\ln t)^2 + b_6 \cdot (\ln t \cdot \ln s) + b_7 \cdot (\ln t \cdot \ln\epsilon) + b_8 \cdot (\ln s)^2 + b_9 \cdot (\ln s \cdot \ln\epsilon) + b_{10} \cdot (\ln\epsilon)^2 \tag{4.25}$$

$$\ln T_1 = c_1 + c_2 \cdot \ln t + c_3 \cdot \ln s + c_4 \cdot \ln\epsilon + c_5 \cdot (\ln t)^2 + c_6 \cdot (\ln t \cdot \ln s) + c_7 \cdot (\ln t \cdot \ln\epsilon) + c_8 \cdot (\ln s)^2 + c_9 \cdot (\ln s \cdot \ln\epsilon) + c_{10} \cdot (\ln\epsilon)^2 \tag{4.26}$$

Regression coefficients of the formulae [4.25] and [4.26] are given in Table 4.2. Figures 4.10 and 4.11 illustrate the quality of the fitting. The simulated values (dashed curves) sometimes show significant variability for smaller pretensions and looser fabrics, which can violate expected monotonic trends

Table 4.2 Coefficients of the regression equations [4.25, 4.26]

	Plain		Twill 2/2		Satin 5/2	
	b	*c*	*b*	*c*	*b*	*c*
1	−9.87	−23.1	−12.1	−17.57	−11.4	−21.0
2	1.86	4.17	2.35	2.96	2.14	3.36
3	0.102	−2.12	−0.381	−0.884	−0.042	−1.72
4	3.01	2.05	2.64	1.68	2.12	6.91
5	−0.10	−0.207	−0.131	−0.192	−0.119	−0.176
6	−0.085	0.111	−0.021	−0.090	−0.062	0.021
7	0.017	−0.100	0.001	0.256	−0.027	−0.150
8	0.028	−0.094	−0.030	−0.113	−0.015	−0.133
9	0.436	0.215	0.367	0.463	0.277	0.557
10	0.435	−0.021	0.263	−0.623	−0.057	−2.52

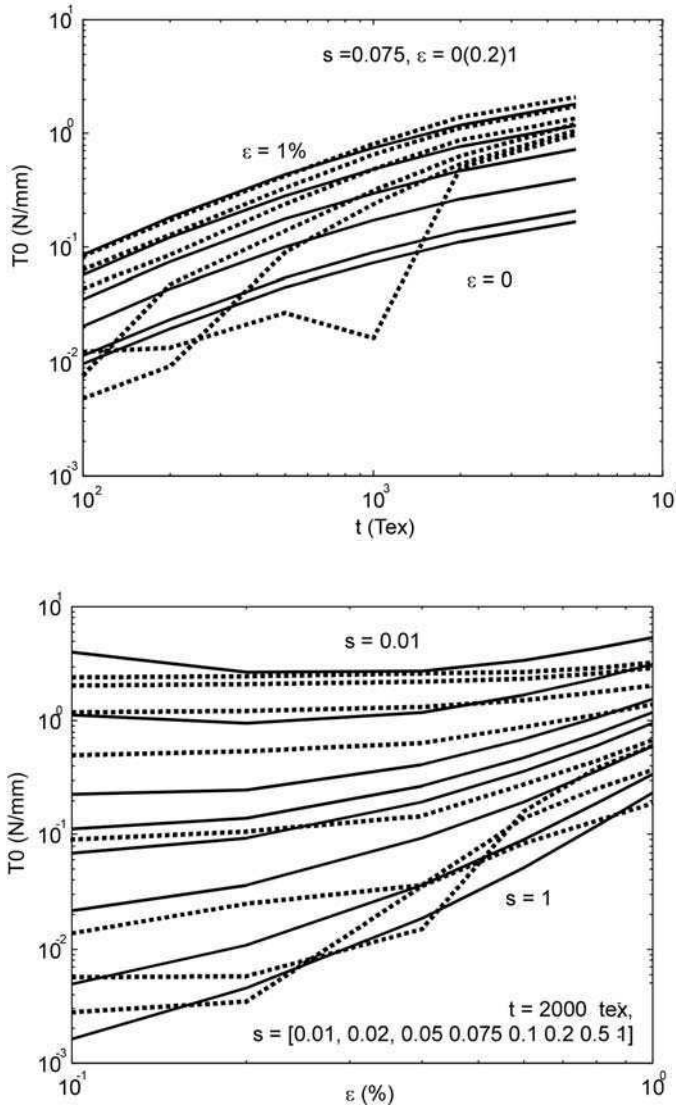

4.10 Examples of the simulated dependencies $T_0 = T_0(t, s, \epsilon)$ (dashed lines) and regression curves [4.25] – solid lines. Plain fabric.

(shear resistance increase with increase of the pre-strain and fabric tightness). These variations are due to the approximate nature of the model and certain instabilities in the iteration loop shown in Fig. 4.4, as well as errors in fitting the diagrams with [4.23]. However, after fitting (therefore smoothening) of the curves they become monotonic and exhibit the expected trends.

Parameterised analytical expressions [4.23–4.26] are ready to use in a user subroutine of forming simulations for woven glass reinforcements.

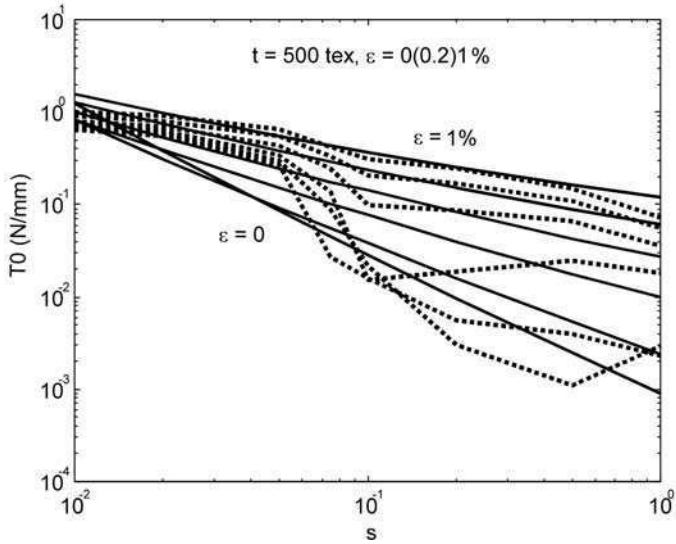

4.10 Continued

4.6.3 Comparison with experiments

Finally, the derived model [4.23–4.26] has to be compared with experimental data. Obtaining input data of the fabric for such a comparison is straightforward: the model requires parameters of the fabric normally provided by the manufacturer: linear density of the yarns, weave structure and ends/pick count (easily transformed into the looseness parameter *s*). Any publication of shear test results contains these data, which allows comparison of the model prediction with published results, without necessary thorough investigation of the fabric internal geometry.

However, the remaining parameter of the model, the pretension of the yarns, is not controlled in most cases of the picture frame test (see Chapter 1). To solve this problem, in cases where the pretension is not given by the experimentalists, an expected range of pretension strain values will be used in the comparison.

Table 4.3 summarises the test cases[22,78] used for the comparison. Apart from the data on the fabric construction, calculations require a value of pretension strain. These data are not readily available. The values given in Table 4.3 were obtained as follows.

In our own measurements[78] we tried to estimate the strain of the fabric in the picture frame measuring the distance between marks on the fabric, made before it had been mounted in the frame and tensed by the wavy grips. This measurement is not precise. The errors, caused by different sources (the main ones being small displacements to be measured and fibrous surface of the yarns, which cause the marks to widen), can be as high as 0.1 to 0.2% of the strain.

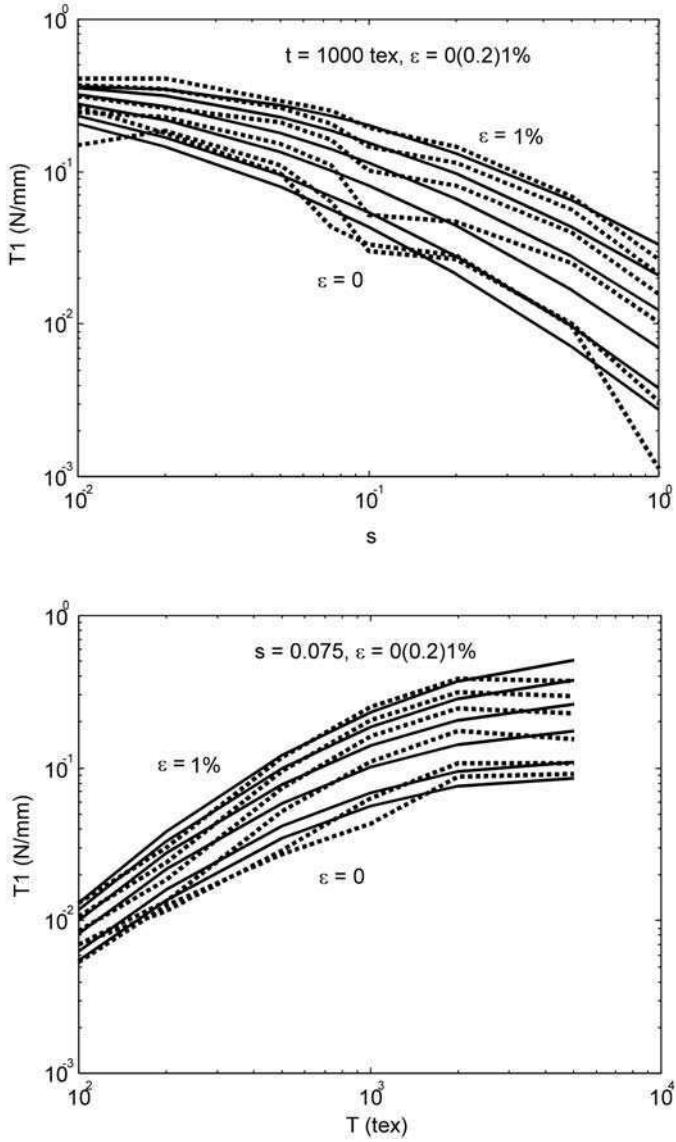

4.11 Examples of the simulated dependencies $T_1 = T_1(t, s, \epsilon)$ (dashed lines) and regression curves [4.26] – solid lines. Twill 2/2 fabric.

Long[22] provides the value of pretension force 1.1 N/mm for fabrics Long-1 and Long-2, and 0.69 N/mm for the fabric Long-3. Calculating the biaxial tensile diagram of the fabrics, using the model described above and input data of Tables 4.2 and 4.3, the pretension was estimated as 0.2% for the fabrics Long-1 (plain weave) and Long-2 (satin), and 0.1% for the twill fabric Long-3.

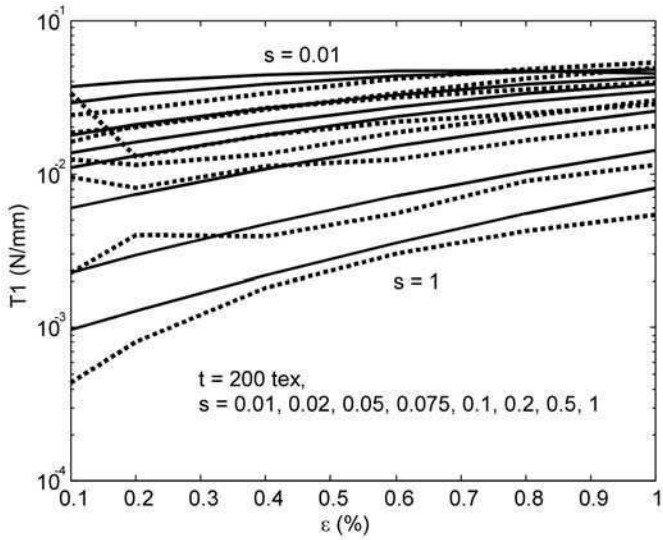

4.11 Continued

The model gives good predictions for the initial stage of shear, up to the locking of the fabric structure (lower estimation of the locking angle is given by a simple geometrical formula, Table 4.3): the set of experimental diagrams for the estimated range of pre-strain agrees well with the calculations (Figs 4.12 and 4.13).

Table 4.3 Input data for comparison with experiments. Data on fabrics 'Lomov' is from ref. 78, 'Long' is from ref. 22

Fabric ID	Weave	Linear density of warp and weft, t, tex	Ends/picks count, yarns/cm	Looseness factors s^*	Geometrical locking angle, °***	Pre-strain, %***
Lomov-1	twill 2/2	280	4.4	0.11	27	first cycle 0.3...0.5, second cycle 0.1...0.3
Lomov-2	plain	480	3.5	0.20	37	first cycle 0.4...0.6, second cycle 0.2...0.4
Lomov-3	plain	1200	2.3	0.29	45	first cycle 0.5...0.7, second cycle 0.3...0.5
Long-1	plain	1220	2.5	0.30	41	0.2
Long-2	satin	1450	2.7	0.32	41	0.2
Long-3	twill 2/2	2500	1.6	0.31	41	0.1

* Value of s is calculated based on *t* value and averaged ends/picks count, using formulae Table 4.1

** Geometrical locking angle $\gamma^* = \arccos\frac{d_2}{p} = \arccos(1 - s)$

*** See text for the explanation of estimation of the pre-strain

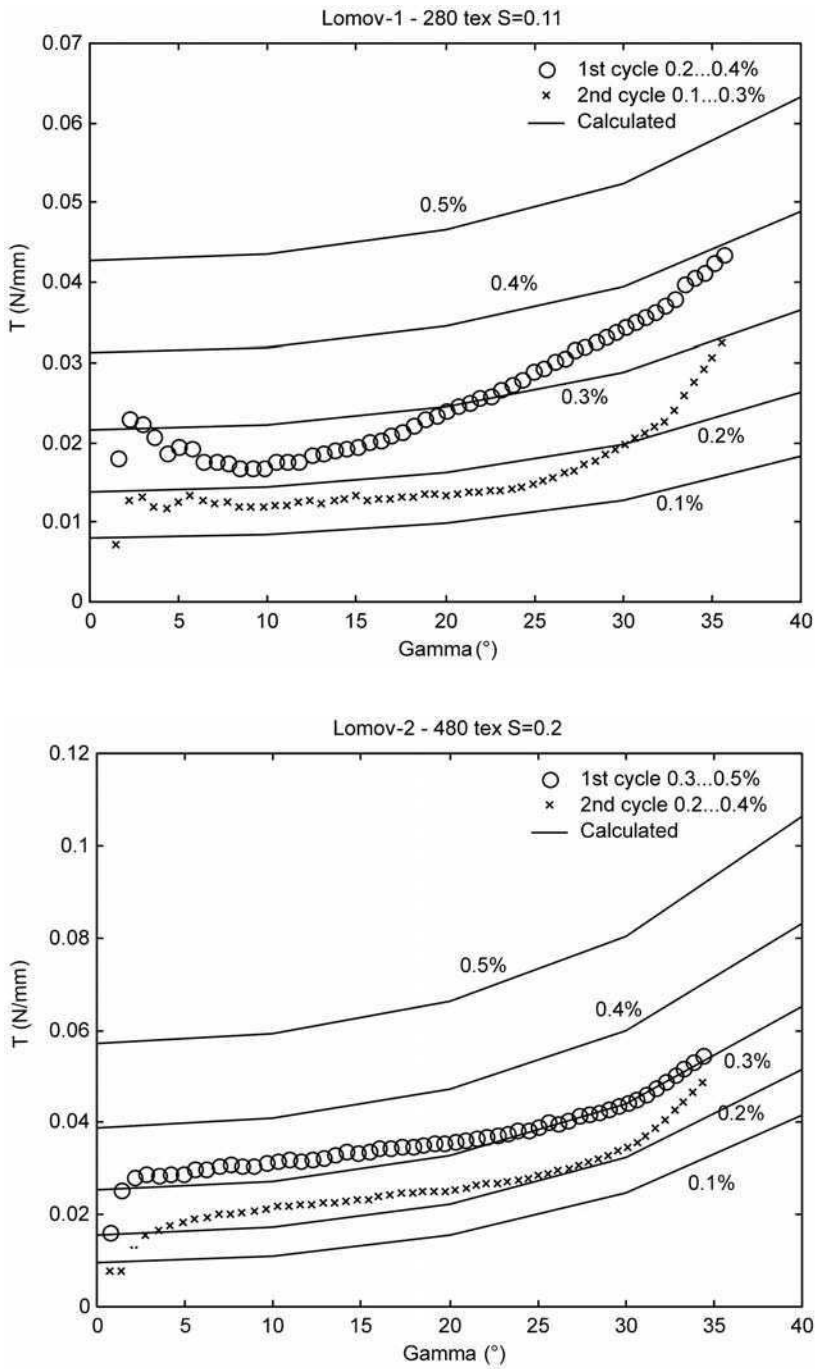

4.12 Comparison between calculated (curves) and experimental (points) data. Fabrics Lomov-1...3.[78]

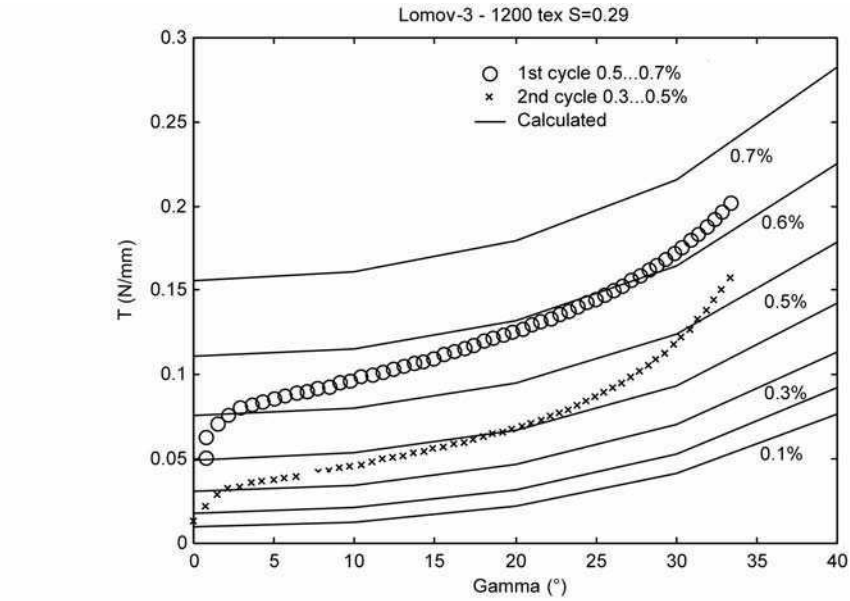

4.12 Continued

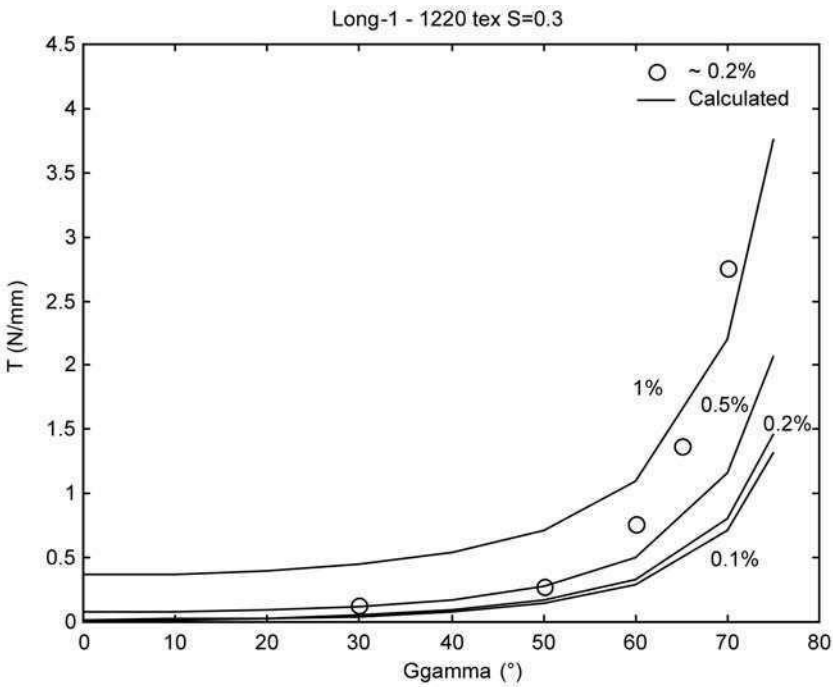

4.13 Comparison between calculated (curves) and experimental (points) data. Fabrics Long-1…3.[22]

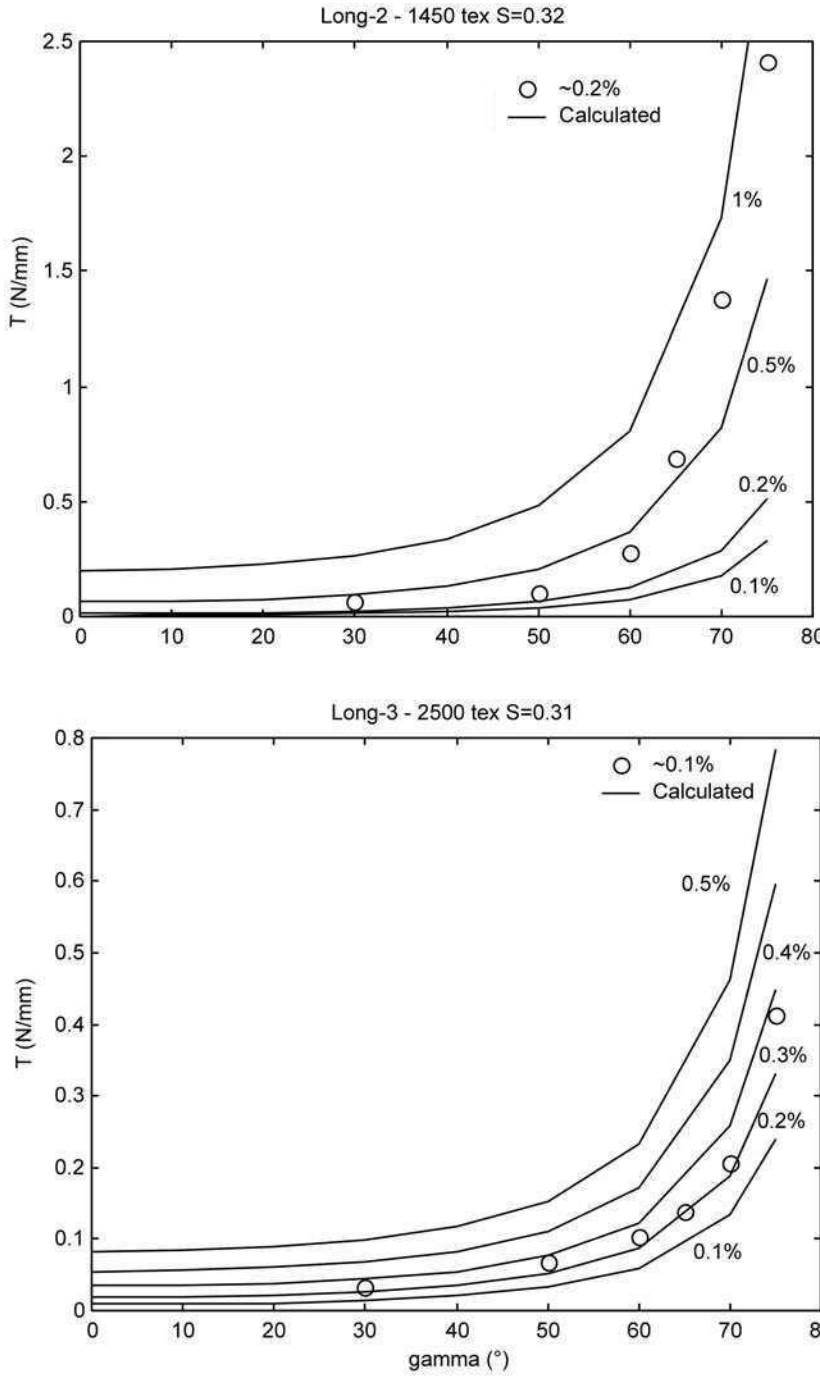

4.13 Continued

After the locking of the structure (distance between the yarns in the sheared fabric equal to the width of the yarns) the sharp increase of the shear resistance is caused by the lateral compression of the yarns. The model accounts for this phenomenon; however, the experimental diagram increases more steeply than the one calculated according to the estimated pre-strain. The discrepancy can be explained by two reasons. First, the 'master' compression curve for the glass rovings (Fig. 4.8d) is defined within a significant scatter of the experimental diagrams; the flattening coefficient is estimated by an approximate formula. These factors determine an approximate nature of the calculation of the lateral compression, employed in the model. Second, for the higher shear one can expect an increase of the tension of the fabric on the frame, which would increase the shear resistance. The experimental diagram intersects calculated iso-strain curves in the direction of increase of the pre-strain.

4.7 Conclusion: creating input data for forming simulations

The theoretical methods described in this chapter and in Chapter 3 provide the possibility to make predictions of the properties of textile reinforcements to be used in forming simulations, producing constitutive descriptions of the materials, as outlined in Chapter 2. The simulations of compressibility can give estimations for the reinforcement thickness (hence fibre volume fraction in the composite) in pressure-controlled resin infusion processes. Coupled shear–biaxial tension simulation provides complex material response surfaces, proposed in refs 32 and 33. Understanding of the scale of the tension-shear coupling effects may help to understand the level of blank-holding forces necessary to eliminate wrinkling.

Being approximate, such predictions are likely to be used for screening of *a priori* unacceptable variants and for qualitative analysis of the manufacturing process. For the latter, several challenges present themselves:

- Tension diagrams of textiles are definitely non-linear. Can a few percent of low-tension strain make a difference for determination of blank-holding conditions?
- Tension in different directions is coupled. Material models available in the existing software packages do not account for this – should they?
- Should the description of shear resistance in forming simulation account for low shear force in the initial stage of shear? For real non-linear behaviour after the geometrical locking angle, or is a simple 'zero resistance – locking – infinite resistance' model sufficient?
- The calculations shown in this chapter demonstrate a strong dependence of the shear resistance on tension. This is not accounted for in the existing forming software – is it necessary to include this effect?

- In general: Does a designer need to spend money, time and resources for complex measurements of non-linear coupled compression-tension-shear behaviour, or it is sufficient to use simpler material models in forming simulations, with the accuracy of predictions enough for practical purposes?

Finally, the 'virtual testing' can help to understand difficulties in non-standardised measurements of biaxial tensile and shear resistance of textiles, and inconsistencies of results obtained under different conditions, as described in Chapter 13, opening the way for standardising the test apparatus and procedures.

4.8 References

1. Lomov, S.V., A.V. Truevtzev and C. Cassidy, A predictive model for the fabric-to-yarn bending stiffness ratio of a plain-woven set fabric. *Textile Research Journal*, 2000. **70**(12) 1088–1096.
2. Sagar, T.V. and P. Potluri, Computation of bending behavior of woven structures using optimization techniques. *Textile Research Journal*, 2004. **74**(10) 879–886.
3. Kawabata, S., M. Niwa and H. Kawai, The finite-deformation theory of plain weave fabrics. Part I. The biaxial-deformation theory. *Journal of the Textile Institute*, 1973. **64**(1) 21–46.
4. Kawabata, S., M. Niwa and H. Kawai, The finite-deformation theory of plain weave fabrics. Part II. The uniaxial-deformation theory. *Journal of the Textile Institute*, 1973. **64**(2) 47–61.
5. Kawabata, S., M. Niwa and H. Kawai, The finite-deformation theory of plain weave fabrics. Part III. The shear-deformation theory. *Journal of the Textile Institute*, 1973. **64**(2) 42–85.
6. de Jong, S. and R. Postle, A general energy analysis in fabric mechanics using optimal control theory. *Textile Research Journal*, 1978. **48**(3) 127–135.
7. Hearle, J.W.S. and W.J. Shanahan, An energy method for calculations in fabric mechanics. *Journal of the Textile Institute*, 1978. **69**(4) 81–110.
8. Komori, T. and M. Itoh, Theory of general deformation of fibre assemblies. *Textile Research Journal*, 1991. **61**(10) 588–594.
9. Anandjiwala, R.D. and G.A.V. Leaf, Large-scale extension and recovery of plain woven fabrics. Part I. Theoretical. *Textile Research Journal*, 1991. **61**(11) 619–634.
10. Anandjiwala, R.D. and G.A.V. Leaf, Large-scale extension and recovery of plain woven fabrics. Part II. Experimental and discussion. *Textile Research Journal*, 1991. **61**(12) 743–755.
11. Huang, N.C., Finite biaxial extension of completely set plain woven fabrics. *Journal of the Applied Mechanics*, 1979. **46**(9) 651–655.
12. Dastoor, P.H., S.P. Hersh, S.K. Batra and W.J. Rasdorf, Computer-assisted structural design of industrial woven fabrics, Part III Modelling of fabric uniaxial/biaxial load deformation. *Journal of the Textile Institute*, 1994. **85**(2) 135–157.
13. Pastore, C.M., A.B. Birger and E. Clyburn, 'Geometrical modelling of textile reinforcements', in *Mechanics of Textile Composites Conference*, 1995, NASA Hampton, Virginia. 597–623.
14. Christoffersen, J., Fabrics orthotropic materials with a stress-free shear mode. *Journal of the Applied Mechanics*, 1980. **47**(1) 71–74.

15. Reumann, R.-D., Neuartiges Berechnungs-verfahren für das flächenstructur-abhängige Kraft-Dehnungs-Verhalten textiler Flächengebilde. *Wissen. Z. Techn. Univ. Dresden*, 1988. **37**(6) 163–169.
16. Chen, B. and T.-W. Chou, Compaction of woven-fabric preforms in liquid composite molding processes single-layer deformation. *Composites Science and Technology*, 1999. **59** 1519–1526.
17. Chen, B. and T.-W. Chou, Compaction of woven-fanric preforms nesting and multi-layer deformation. *Composites Science and Technology*, 2000. **60** 2223–2231.
18. Chen, B., A.H.-D. Cheng and T.-W. Chou, A nonlinear compaction model for fibrous preforms. *Composites Part A*, 2001. **32** 701–707.
19. Chen, B., E.J. Lang and T.-W. Chou, Experimental and theoretical studies of fabric compaction behaviour in resin transfer moulding. *Materials Science and Engineering*, 2001. **A317** 188–196.
20. Kurashiki, T., M. Zako and I. Verpoest, 'Damage development of woven fabric composites considering an effect of mismatch of lay-up', in *Composites for the Future, Proceedings 10th European Conference on Composite Materials (ECCM-10)*, 2002 Brugge. CD edition.
21. Lomov, S.V. and I. Verpoest, Compression of woven reinforcements a mathematical model. *Journal of Reinforced Plastics and Composites*, 2000. **19**(16) 1329–1350.
22. Long, A., 'Process modelling for textile composites', in *International Conference on Virtual Prototiping EUROPAM 2000*. 2000 Nantes. 1–17.
23. Long, A.C., M.J. Clifford, P. Harrison and C.D. Rudd, 'Modelling of draping and deformation for textile composites', in *ICMAC – International Conference for Manufacturing of Advanced Composites*. 2001, IOM Communications Belfast. 66–76.
24. Long, A.C., F. Robitaille, B.J. Souter and C.D. Rudd, 'Permeability Prediction for Sheared, Compacted Textiles During Liquid Composite Modelling', in *13th International Conference on Composite Materials (ICCM-13)*. 2001. Beijing, China.
25. Crookston, J.J., A.C. Long and I.A. Jones, Modelling effects of reinforcement deformation during manufacture on elastic properties of textile composites. *Plastics, Rubber and Composites*, 2002. **31**(2) 58–65.
26. Harrison, P., J. Wiggers, A.C. Long and C.D. Rudd, 'Constitutive modelling based on meso and micro kinematics for woven and stitched fabrics', in *Proceedings ICCM-14*. 2003 San Diego. CD edition.
27. Harrison, P., M.J. Clifford, A. Long and C.D. Rudd, A constituent-based predictive approach to modelling the rheology of viscous textile composites. *Composites Part A*, 2004. **35** 915–931.
28. Harrison, P., M.J. Clifford and A.C. Long, Shear cheracterisation of viscous woven textile composites A comparison between picture frame and bias extension experiments. *Composites Science and Technology*, 2004. **64** 1453–1465.
29. Liu, L., J. Chen and J.A. Sherwood, Two-dimensional macro-mechanics shear models of woven fabrics. *Composites Part A*, 2004. **36** 105–114.
30. Boisse, P., M. Borr, K. Buet and A. Cherouat, Finite element simulations of textile composite forming including the biaxial fabric behaviour. *Composites Part B*, 1999. **28B** 453–464.
31. Boisse, P., A. Cherouat, J.C. Gelin and H. Sabhi, Experimenal study and finite element simulation of a glass fibre fabric shaping process. *Polymer Composites*, 1999. **16**(1) 83–95.

32. Boisse, P., K. Buet, A. Gasser and J. Launay, Meso/macro-mechanical behaviour of textile reinforcements for thin composites. *Composites Science and Technology*, 2001. **61** 395–401.
33. Boisse, P., A. Gasser and G. Hivet, Analyses of fabric tensile behaviour determination of the biaxial tension-strain surfaces and their use in forming simulations. *Composites Part A*, 2001. **32**(10) 1395–1414.
34. Gasser, A., P. Boisse and S. Hanklar, Analysis of the mechanical behaviour of dry fabric reinforcements. 3D simulations versus biaxial tests. *Computational Materials Science*, 2000. **17** 7–20.
35. Launay, J., K. Buet-Gautier, G. Hivet and P. Boisse, Analyse experimentale et modeles pour le comportement mechanique biaxial des renforts tisses de composites. *Revue des composites et des materiaux avances*, 1999. **9**(1) 27–55.
36. Kuwazuru, O. and N. Yoshikawa, 'Non-constitutive numerical modeling for plain-weave fabrics', in *Proceedings of 7th Japan International SAMPE Symposium & Exhibition, November 13–16*. 2001 Tokyo. 729–732.
37. Sakakibara, K., A. Yokoyama and H. Hamada, 'Deformation mechanism of textile under uni- and biaxial tensile loading', in *Proceedings of 7th Japan International SAMPE Symposium & Exhibition, November 13–16*. 2001 Tokyo. 705–708.
38. Zouari, B., F. Dumont, J.L. Daniel and P. Boisse, 'Analyses of woven fabric shearing by optical method and implementation in a finite element program', in *Proceedings of the 6th ESAFORM Conference on material Forming*. 2003 Salerno. 875–887.
39. Hivet, G., B. Laine and P. Boisse, 'Consistent preprocessor for the unit woven cell for meso-macro analyses of fabric forming', in *Procedings of the 8th ESAFORM Conference on Material Forming*. 2005 Cluj-Napoca. 947–950.
40. Kondratiev, S., *Finite element modelling of the spatial stress-strain state of textiles and textile composites*. Masters thesis, 2001, State Technical University St.-Petersburg.
41. Van Genechten, B., *Finite element modelling of textile composites*. Masters thesis, 2002, Vrije Universiteit Brussel – Katholieke Universiteit Leuven.
42. Robitaille, F., A.C. Long, I.A. Jones and C.D. Rudd, Authomatically generated geometric descriptions of textile and composite unit cells. *Composites Part A*, 2003. **34**(4) 303–312.
43. Robitaille, F., A. Long, M. Sherburn, C.C. Wong and C. Rudd, 'Predictive modelling of processing and performance properties of textile composite unit cells current status and perspectives', in *Proceedings ECCM-11*. 2004. CD Edition.
44. Lomov, S.V., I. Verpoest, E. Bernal, F. Boust, V. Carvelli, J.-F. Delerue, P. De Luka, L. Dufort, S. Hirosawa, G. Huysmans, S. Kondratiev, B. Laine, T. Mikolanda, H. Nakai, C. Poggi, D. Roose, F. Tumer, B. van den Broucke, B. Verleye and M. Zako, 'Virtual textile composites software Wisetex integration with micro-mechanical, permeability and structural analysis', in *Proceedings of the 15th International Conference on Composite Materials (ICCM-15)*. 2005 Durban. CD edition.
45. Lomov, S.V., X. Ding, S. Hirosawa, S.V. Kondratiev, J. Molimard, H. Nakai, A. Vautrin, I. Verpoest and M. Zako, 'FE simulations of textile composites on unit cell level validation with full-field strain measurements', in *Proceedings 26th SAMPE-Europe Conference*. 2005 Paris. 28–33.
46. Verpoest, I. and S.V. Lomov, Virtual textile composites software Wisetex integration with micro-mechanical, permeability and structural analysis. *Composites*

Science and Technology, 2005, **65** (15–16) 2563–2574.
47. Mikolanda, T., S.V. Lomov, M. Kosek and I. Verpoest, *Simple use of virtual reality for effective visualization of textile material structures*, *CODATA Prague Workshop Information Visualization, Presentation, and Design*, 2004, Prague. CD edition.
48. Lomov, S.V., E. Bernal, D.S. Ivanov, S.V. Kondratiev and I. Verpoest, Homogenisation of a sheared unit cell of textile composites FEA and approximate inclusion model. *Revue européenne des éléments finis*, **14**(6–7) 709–728.
49. Lomov, S.V., G. Huysmans, Y. Luo, R. Parnas, A. Prodromou, I. Verpoest and F.R. Phelan, Textile Composites Modelling Strategies. *Composites Part A*, 2001. **32**(10) 1379–1394.
50. Belov, E.B., S.V. Lomov, I. Verpoest, T. Peeters, D. Roose, R.S. Parnas, K. Hoes and V. Sol, Modelling of permeability of textile reinforcements Lattice Boltzmann method. *Composites Science and Technology*, 2004. **64** 1069–1080.
51. Lomov, S.V., A.V. Gusakov, G. Huysmans, A. Prodromou and I. Verpoest, Textile geometry preprocessor for meso-mechanical models of woven composites. *Composites Science and Technology*, 2000. **60** 2083–2095.
52. Lomov, S.V., I. Verpoest, T. Peeters, D. Roose and M. Zako, Nesting in textile laminates geometrical modelling of the laminate. *Composites Science and Technology*, 2002. **63**(7) 993–1007.
53. Lomov, S.V., G. Huysmans and I. Verpoest, Hierarchy of textile structures and architecture of fabric geometric models. *Textile Research Journal*, 2001. **71**(6) 534–543.
54. Lomov, S.V., A. Nakai, R.S. Parnas, S. Bandyopadhyay Ghosh and I. Verpoest, Experimental and theoretical characterisation of the geometry of flat two- and three-axial braids. *Textile Research Journal*, 2002. **72**(8) 706–712.
55. Lomov, S.V., T. Truong Chi, I. Verpoest, T. Peeters, V. Roose, P. Boisse and A. Gasser, Mathematical modelling of internal geometry and deformability of woven preforms. *International Journal of Forming Processes*, 2003. **6**(3-4) 413–442.
56. Lomov, S.V., B. Van den Broucke, F. Tumer, I. Verpoest, P. De Luka and L. Dufort, 'Micro-macro structural analysis of textile composite parts', in *Proceedings ECCM-11*. 2004 Rodos. CD Edition.
57. Van den Broucke, B., F. Tumer, S.V. Lomov, I. Verpoest, P. De Luka and L. Dufort, 'Micro-macro structural analysis of textile composite parts case study', in *Proceedings of the 25th International SAMPE Europe Conference, March 30th–April 1st*. 2004 Paris. 194–199.
58. Lomov, S.V. and B.M. Primachenko, Mathematical modelling of two-layered woven fabric under tension. *Technologia Tekstilnoy Promyshlennosty*, 1992(1) 49–53.
59. Lomov, S.V., Computer aided design of multilayered woven structures, part 1. *Technologia Tekstilnoy Promyshlennosty*, 1993(1) 40–45.
60. Lomov, S.V., Computer aided design of multilayered woven structures, part 2. *Technologia Tekstilnoy Promyshlennosty*, 1993(2) 47–50.
61. Primachenko, B.M., S.V. Lomov, V.V. Lemeshkov, O.P. Petrova and D.P. Pizvanova, Computer aided design of multilayered woven structures, part 3. *Technologia Tekstilnoy Promyshlennosty*, 1993(3) 42–45.
62. Lomov, S.V. and A.V. Gusakov, Modellirung von drei-dimensionalen gewebe Strukturen. *Technische Textilen*, 1995. **38** 20–21.
63. Lomov, S.V. and N.N. Truevtzev, A software package for the prediction of woven fabrics geometrical and mechanical properties. *Fibres & Textiles in Eastern Europe*,

1995. **3**(2) 49–52.
64. Lomov, S.V., I. Verpoest and F. Robitaille, 'Manufacturing and internal geometry of textiles', in *Design and manufacture of textile composites*, A. Long, Editor. 2005, Woodhead Publishing Ltd. 1–60.
65. Parnas, R.S., J.G. Howard, T.L. Luce and S.G. Adwani, Permeability characterisation. Part 1 A proposed standard reference fabric for permeability. *Polymer Composites*, 1995. **16**(6) 429–445.
66. Olofsson, B., A general model of a fabric as a geometric-mechanical structure. *Journal of the Textile Institute*, 1964. **55**(11) T541–T557.
67. Daniel, J.L., D. Soulat and P. Boisse, 'Shear and tension stiffness influence in composites forming modelling', in *Proceedings ESAFORM-2004*. 2004 Trondheim. 301–304.
68. Lomov, S.V. and I. Verpoest, Model of shear of woven fabric and parametric description of shear resistance of glass woven reinforcements. *Composites Science and Technology*, 2006. **66** 919–933.
69. Peng, X.Q., J. Cao, J. Chen, P. Xue, D.S. Lussier and L. Liu, Experimental and numerical analysis on normalisation of picture frame tests for composite materials. *Composites Science and Technology*, 2004. **64**(1) 11–21.
70. Harrison, P., M.J. Clifford, A.C. Long and C.D. Rudd, 'A micro-mechanical approach to stress-prediction during shear for woven continuous fibre-reinforced impregnated composites', in *Proceedings of the 5th International ESAFORM Conference on Material Forming*, 2002 Krakow. 275–278.
71. Lomov, S.V., A. Willems, M. Barburski, T. Stoilova and I. Verpoest, 'Strain field in the picture frame test large and small scale optical measurements', in *Proceedings of the 8th ESAFORM Conference on Material Forming*. 2005 Cluj-Napoca. 935–938.
72. Leaf, G.A.V. and A.M.F. Sheta, The initial shear modulus of plain-woven fabrics. *Journal of the Textile Institute*, 1984. **75**(3) 157–183.
73. Lomov, S.V., 'Prediction of geometry and mechanical properties of woven technical fabrics with mathematical modelling', in *Dept. Mechanical Technology of Fibrous Materials*. 1995, SPbSUTD St. Petersburg.
74. Belov, E.B., S.V. Lomov, N.N. Truevtsev, M.S. Bradshaw and R.J. Harwood, Study of yarn snarling. Part I Critical parameters of snarling. *Journal of the Textile Institute, Part 1 Fibre Science and Textile Technology*, 2002. **93**(4) 341–365.
75. Morton, W.E. and D.W.S. Hearle, *Physical properties of textile fibres*, The Textile Institute, Manchester, 1993.
76. Lomov, S.V., G. Huysmans, Y. Luo, A. Prodromou, I. Verpoest and A.V. Gusakov. 'Textile geometry preprocessor for meso-mechanical and permeability modelling of textile composites', in *9th European Conference on Composite Materials (ECCM-9)*. 2000. Brighton IOM Communications.
77. Verpoest, I., G. Huysmans, Y. Luo, R.S. Parnas, A. Prodromou and S.V. Lomov, 'An integrated modelling strategy for processing and properties of textile composites', in *Proceedings of the 46th International SAMPE symposium and exhibition May 6th–10th*. 2001 Long Beach, California. 2472–2483.
78. Lomov, S.V., A. Willems, I. Verpoest, Y. Zhu, M. Barburski and T. Stoilova, Picture frame of woven fabrics with a full-field strain registration. *Textile Research Journal*, 2006. **76**(3) 243–252.